Sensors & Transducers, Vol. 160, Issue 12, December 2013, pp. 163-171

www.sensorsportal.com

Sensors & Transducers

© 2013 by IFSA

http://www.sensorsportal.com

Acoustic Emission Mechanism and Source Modeling of Dynamic Crack Detection in Steel Structure

Li LI, Ji LI, Baojia CHEN

A Hubei Key Laboratory of Hydroelectric Machinery Design & Maintenance,
China Three Gorges University, Yichang, Hubei, 443002, China
E-mail: 13339786801@189.cn

Received: 4 September 2013 /Accepted: 22 November 2013 /Published: 30 December 2013

Abstract: Cracks are dangerous and frequently observed defects in steel structures. Therefore, the understanding of the mechanism of crack is very important to structure safety. Although the mechanism of static crack has been widely studied by researchers, the mechanism of dynamic crack has been left out and seldom been discussed. In this paper, a modeling method for acoustic emission (AE) source of dynamic crack was proposed for the mechanism revelation. In the method, AE signal was related to crack stress based on the theory of elasto-dynamics; the crack stress was inversely modeled from AE signal by employing half-space Green's function and de-convolution procedure. When the method was applied to an AE testing for dynamic crack in steel structure, AE source function representing the time history of crack stress was obtained. The crack stress was found to be a step-like function with a pulse, and with it the mechanism and transient dynamic process of crack growth (crack initiation and propagation) was recovered. The results indicated that, the modeling method is effective for the study on the mechanism of dynamic crack. *Copyright © 2013 IFSA.*

Keywords: Acoustic emission, Modeling, Dynamic crack, Steel structure, Mechanism.

1. Introduction

Cracks are dangerous and frequently observed defects in steel structures such as cranes and oil drilling platforms. They are formed in a material for many causes, and may expand and finally lead to catastrophic failures of steel structures. Therefore, understanding of the mechanism of crack is necessary for fail-safe design of structural components made of steel. Recent years, many efforts have been made in the mechanism research on crack, among which mainly two approaches were tracked. They are both on the same basis of linear elastic fracture mechanics (LEFM). The first approach was in the continuity of the pioneer works of Griffith and Irwin. And it was based on the local stress intensity factors (K_I, K_{II}, K_{III}) and energy release rate calculation near crack tip. The second approach was developed employing energy variational minimization and phase-field analysis in the crack zone [1]. Both of them aim at predicting initiation and propagation conditions (loading, path) of static crack; and they have been proved to be effective for the static problems. However, in the case of dynamic problems, for instance, description of the mechanism of dynamic crack, a new approach is urgently needed.

Nowadays, in order to explore the mechanism related to dynamic crack, many researchers begin to pay more attention to acoustic emission (AE) testing technique, since AE testing is very sensitive to crack initiation and propagation i.e. crack growth. At the transient of crack growth, the elastic strain energy, stored within a material under load, is released. One part of it radiates from the region of cracking in the

form of elastic waves. In AE testing, the elastic waves reaching the surface of a body can be detected by sensitive transducers and recorded as AE signals. Many studies have shown that AE signals can be a sensitive function of material properties [2-5]. From AE signals a lot of information about the dynamic behavior of crack can be extracted. Some of AE parameters extracted from AE signals have been used in dynamic crack characterization. For instance, AE energy has been used to determine the critical energy release rate; frequency counts have been used to distinguish various failure modes occurring at different loading stages; the rate and sum of occurrence of AE activity have been used to predict the extent of internal damage of material [6]. These applications have shown the latent capacity of AE testing in dynamic crack characterization, however, in the aspect of mechanism description, further AE signal analysis is necessary.

AE waveform is essentially an elastic wave emitted from an AE source. Starting from this point, researchers attempted to explain AE wave motion using the theory of elasto-dynamics. This was done both theoretically and experimentally by Breckenridge in the first place, based on the prior work of Lamb and Perkeris [7]. In his study, AE signal excited by a vertical point loading applied suddenly onto the surface of an elastic half-space was theoretically estimated. Subsequently in his famous experiment, a glass capillary was break on a steel block to simulate a point-step force applied onto the material and an AE signal was measured. The measured AE signal was found to agree well with that estimated using the solution of Lamb's problem. Breckenridge's study was then boosted by Michaels, Ohtsu, et al [8-11]. With their contribution, a de-convolution procedure was developed and an AE source function representing the force time history was obtained.

In this paper, a modeling method for AE source of dynamic crack is proposed for the mechanism description, following the study of Michaels and Ohtsu. In the method, the variation in crack stress (traction on the crack surface) is related to AE signal based on elasto-dynamic theory and characterized by AE source function. And AE source functions were inversely modeled from AE signal by employing Green's function in the half-space and the de-convolution procedure. Applying the method to AE testing for a simulated dynamic crack in a steel structure, AE source functions describing the time history of crack stress were modeled. The obtained AE source functions were then discussed in detail to represent the mechanism of dynamic crack clearly in the aspect of crack stress variation. The paper is organized as follows. In Sec. II, a set of equations are presented to give a general explanation of elasto-dynamic theory and de-convolution procedure for AE source function modeling; in Sec. III, an AE testing for dynamic crack in steel structure is demonstrated; and finally in Sec. IV, the obtained AE source function and the mechanism is discussed in detail.

2. Theory

2.1. Navier's Equations of Elasto-dynamics

According to the theory of elasto-dynamics, any behavior (for example crack initiation or propagation) of disturbance in the elastic medium at point $\mathbf{x}'$ and time τ would cause displacements $u_i(\mathbf{x},t)$ at point $\mathbf{x}$ and time t. The displacements initially at rest in the elastic body Ω can be expressed as the sum of the contributions of the body forces F_j distributed in Ω, the surface tractions T, and the surface displacements u_Σ on the boundary Σ of the body. It is also proved that the surface tractions and displacements can be treated as equivalent body forces distributed over the boundary. For a uniform elastic medium and a Cartesian co-ordinate system, the displacement $u_i(\mathbf{x},t)$ satisfies the equation for the conservation of linear momentum, i.e. Navier's equation which can be written as,

$$\begin{aligned}\rho\ddot{u}_i(\mathbf{x},t) = f_i(\mathbf{x},t) + (\lambda+\mu)u_{j,ij}(\mathbf{x},t) \\ + \mu u_{i,jj}(\mathbf{x},t)\end{aligned}, \quad (1)$$

where summation over repeated indices is used, commas indicate partial differentiation and dot notation indicates partial differentiation with respect to time. ρ is the density; λ, μ are the Lamé constants; f_i is the source of the elastic disturbance, which is the sum of the actual body forces and the equivalent body forces of surface tractions and displacements. Eq. (1) represents a statement of dynamic equilibrium in each of three orthogonal directions. It is the governing equation of elasto-dynamics and can be solved both analytically and numerically.

2.2. The Green's Function Method

Green's function is a well-defined analytical tool to solve the second order system of coupled linear partial differential equations. For wave motion excited by an impulsive (i.e. delta function) body force concentrated at $(\mathbf{x}',\tau)$ and acting in the k-th direction, Eq. (1) can be written as.

$$\begin{aligned}\rho G_{ik}(\mathbf{x},t;\mathbf{x}',\tau) = \delta_{ik}\delta(\mathbf{x}-\mathbf{x}')\delta(t-\tau) \\ + (\lambda+\mu)G_{jk,ji}(\mathbf{x},t;\mathbf{x}',\tau), \\ + \mu G_{ik,jj}(\mathbf{x},t;\mathbf{x}',\tau)\end{aligned} \quad (2)$$

where the bodies dynamic elastic Green's tensor is denoted by $G_{ik}(\mathbf{x},t;\mathbf{x}',\tau)$. It represents displacement in the i-th direction at $(\mathbf{x},t)$ due to a unit strength impulsive body force concentrated at $(\mathbf{x}',\tau)$ and

acting in the k -th direction. δ_{ik} is the Kronecker delta while $\delta(\mathbf{x}-\mathbf{x}')$ and $\delta(t-\tau)$ are Dirac delta functions. Note that the Green's tensor satisfies both homogeneous boundary conditions, a quiescent past.

Using Betti's reciprocal theorem, the time-dependent displacement $u_i(\mathbf{x},t)$ at $(\mathbf{x},t)$ on or within the body due to wave motion excited by application of body forces at $(\mathbf{x}',\tau)$ is obtained by convolution of the body force distribution with the appropriate Green's tensor. In practice, point responses due to Heaviside time dependent sources are used to avoid singularities in $G_{ij}(\mathbf{x},t;\mathbf{x}',\tau)$ which can cause difficulties in computing, manipulating and presenting results. The Dirac delta function $\delta(\tau)$ and the Heaviside function $H(\tau)$ can be related by differentiation with respect to time

$$\delta(\tau)=\frac{\mathrm{d}}{\mathrm{d}t}H(\tau), \tag{3}$$

Substituting Eq. (3) into Eq. (2) and integrating with respect to time t allow definition of the Heaviside response $G_{ij}^{H}(\mathbf{x},t;\mathbf{x}',\tau)$

$$G_{ij}(\mathbf{x},t;\mathbf{x}',\tau)=\frac{\mathrm{d}}{\mathrm{d}t}G_{ij}^{H}(\mathbf{x},t;\mathbf{x}',\tau), \tag{4}$$

Through Eqs. (2) and (4), reciprocal theorem and integration by parts of it follows that

$$u_i(\mathbf{x},t)=\int_0^t\int_\Omega G_{ij}^{H}(\mathbf{x},t;\mathbf{x}',t-\tau)\dot{f}_j(\mathbf{x}',t)\,\mathrm{d}t\mathrm{d}\Omega, \tag{5}$$

Eq. (5) is a generalized relationship between body force and the displacement of elastic wave motion. In this paper, one simple case shown in Fig. 1 will be discussed. In Fig. 1, if a force is applied in direction x_3 on the boundary of a half-space and the normal displacement is detected on the surface. Eq. (5) can be simplified into two-dimension as,

$$u_i(\mathbf{x},t)=\int_S \dot{f}_j(\mathbf{x}',\tau)*G_{ij}^{H}(\mathbf{x},t;\mathbf{x}',\tau)\,dS, \tag{6}$$

where S is the area of the force applied and $*$ represents convolution.

When the area is much smaller compared with the elastic wave length, the force applied could be regarded as a point force. Then, Eq. (6) could be simplified into a convolution relating point force f in direction x_3 to point detection u in direction x_3, expressed as

$$\begin{aligned}u(\mathbf{x},t)&=u_3(\mathbf{x},t)=f_3(\mathbf{x}',\tau)*G_{33}(\mathbf{x},t;\mathbf{x}',\tau)\\&=\dot{f}(\mathbf{x}',\tau)*G_{33}^{H}(\mathbf{x},t;\mathbf{x}',\tau)\\&=\dot{f}(\mathbf{x}',\tau)*G(\mathbf{x},t;\mathbf{x}',\tau)\end{aligned}, \tag{7}$$

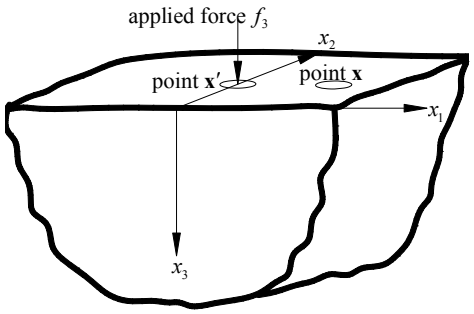

Fig. 1. Sketch for the two-dimension case.

where $G=G_{33}^{H}$ and $f=f_3$.

The Green's function due to a Heaviside function force for a half space was numerically evaluated by Perkeris [7], and could be expressed as follows

$$G(t)=\begin{cases}0, & t<\dfrac{r}{\kappa v_s}\\[2ex]\dfrac{\kappa^2}{\pi^2\mu r}\Pr\displaystyle\int_{1/\nu}^{tv_s/r}\frac{\xi\left(1-2\xi^2\right)^2\sqrt{\xi^2-1/\kappa^2}}{g(\xi)\sqrt{(tv_s/r)^2-\xi^2}}d\xi, & \dfrac{r}{\kappa v_s}<t<\dfrac{r}{v_s}\\[2ex]\dfrac{\kappa^2}{\pi^2\mu r}\Pr\displaystyle\int_{1}^{tv_s/r}\frac{4\xi^3\left(\xi^2-1/\kappa^2\right)\sqrt{\xi^2-1}}{g(\xi)\sqrt{(tv_s/r)^2-\xi^2}}d\xi, & t>\dfrac{r}{v_s}\end{cases} \tag{8}$$

where r is the distance from the detection point $\mathbf{x}$ to the source position $\mathbf{x}'$; μ is Lamé constant; ν is Poisson ratio; and the velocity of primary wave and secondary waves are v_p and v_s, respectively; and κ denotes velocity ratio.

$$\kappa=\frac{v_p}{v_s}, \tag{9}$$

Pr designates principal value of the integral with

$$\begin{aligned}&g(\xi)\\&=\kappa^2-8\kappa^2\xi^2+8\xi^4\left(3\kappa^2-2\right)-16\xi^6\left(\kappa^2-1\right)\end{aligned}, \tag{10}$$

2.3. Modeling of AE Source Function

In practical application, since the transducer employed had a fairly flat response in the detecting frequency range and the resonant frequency was at 1 MHz, the physical quantities of AE signals detected through our monitoring system are considered as vertical accelerations at the free surface. Then the recorded signal can be represented as

$$V(t)=\frac{d^2u(t)}{dt^2}=\frac{d^2}{dt^2}\left[\frac{df(t)}{dt}*G(t)\right], \quad (11)$$
$$=\frac{d^3f(t)}{dt^3}*G(t)$$

The AE source function can be modeled from the measured voltage $V(t)$ and the Green's function under de-convolution procedure,

$$\frac{d^3f(t)}{dt^3}=V(t)*\left[G(t)\right]^{-1}, \quad (12)$$

where $\left[G(t)\right]^{-1}$ is the inverse function of $G(t)$. Then the AE source function can be represented by integral,

$$f(t)=\int V(t)*\left[G(t)\right]^{-1}\mathrm{d}t, \quad (13)$$

Eqs. (12) and (13) are the inverse and forward relation between the detected AE signal and AE source function, respectively

3. Experimentations

3.1. AE Testing Instrumentation

The piezoelectric sensor was used to capture vertical accelerations on the structure surface. The transducer had a flat-frequency range 0.1~1 MHz, and dimensions of 17 mm in height and 16mm in diameter. The sensor output was amplified by a preamplifier of 40 dB. A PCI-2 system of PAC was used for data acquisition. Signals were captured and recorded through a 20~100 kHz band pass filter so that the low- and high- frequency noises should be eliminated. It has been found that the influence of this filter on the early time response of original signal is sufficiently small to make precise signal analysis. Signals with duration of 409.6 μsec were recorded at the sampling interval of 0.1 μsec for subsequent analysis.

3.2. AE Testing for Dynamic Crack

Experiment measurements were made on the surface of a thick steel structure. Dimensions of the structure were 377×260×50 mm^3 (span×height× thickness), as shown in Fig. 2 (a). These dimensions were selected so that a suitable length of signal could be recorded before reflections from structure boundaries would contaminate the signal. Material properties of the structure were listed in Table 1.

2B Pencil leads in different diameters were used as dynamic crack simulators. The pencil leads were broken on the structure surface, 20 mm away from the transducer, to simulate crack initiation and propagation in the structure. The pencil leads were shown in Fig. 2.(b), and were numbered consecutively as S_1, S_2, S_3, among which S_1 was a sharp tip of 0.3 mm, S_2, S_3 were round rods of 0.5 mm and 0.7 mm, respectively. At least 2 events were recorded during each test, and only the first ones were accepted because the initial arrival of energy was unambiguously present in the first records.

Table 1. Properties of structure material.

Property	Value
Density ρ	7780 kg/m^3
Poisson's ratio ν	0.211
Rigidity μ	7.845×1010 N/m
Young's modulus E	19×1010 Pa
P- wave velocity v_p	5254 m/s

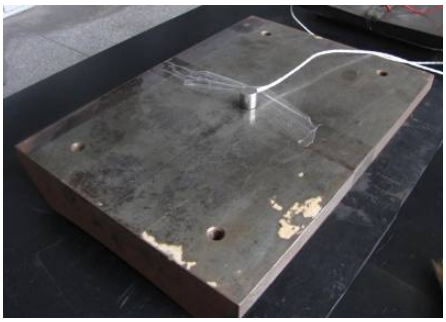

(a)

(b)

(c)

Fig. 2. AE testing for crack initiation and propagation in structure (a) Steel structure and the transducer mounted on the surface, (b) Dynamic crack simulators in different diameters, and (c) Dynamic crack simulating.

4. Mechanisms

4.1. "Early part" Determination

The AE signals from simulated dynamic cracks were detected on the surface of the steel structure, and presented in Fig. 3. In each signal, only the "early part" including several initial arrivals is definitely from the dynamic crack with no boundary reflection components. Thus, "early part" is effective for the analysis of dynamic cracks and it should be firstly determined so that the AE source function can be modeled to recover the mechanism of dynamic cracks.

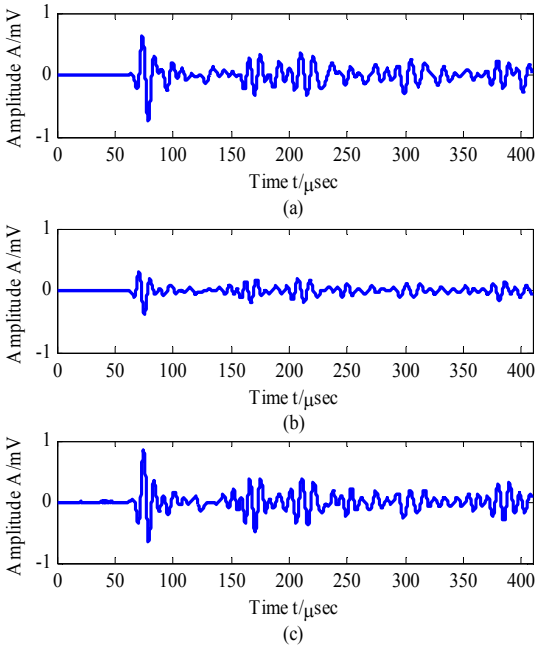

Fig. 3. Detected AE signals from (a) S_1, (b) S_2, and (c) S_3.

4.1.1. Time Series Analysis of First Arrivals

Several first arrivals of the signal of S_1 are shown in Fig. 4. In the figure, the first arrival point is denoted by A_0; the first five arrivals are marked by V_i for valley and P_i for peak. Starting from A_0, the arrival comes to the valley V_1 firstly; then jumps to P_1 rapidly; after that goes to V_2 and P_2 in turn; and ends up with the valley V_3. The amplitudes of V_1, V_3 exhibit to be smaller than V_2, and the amplitude of P_1 is shown to be bigger than P_2. This trace was tracked by all three signals shown in Fig. 3, which leads to a good agreement in the shapes of signals at the initial part. However, this agreement in the shape of waveforms is not observed after the first five arrivals.

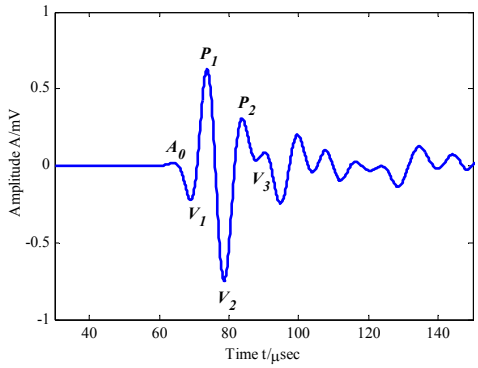

Fig. 4. Signal from S_1 within the time interval of 30~150 μsec.

4.1.2. Frequency Analysis Based on STFT

Short Time Fourier Transform (STFT) is a powerful tool for non-stationary signal for example AE signal [12]. It transforms a signal into a time-frequency representation and gives localized information such as energy scattering of the signal. In this paper, the theory of STFT will not be presented in detail. The signals from S_1, S_2, S_3 were analyzed using STFT method and the time-frequency representations were shown in Fig. 5. From Fig. 5, it can be found that the energy of all three AE signals at initial part concentrates on the first arrivals with duration of about 20 μsec from the first arrival point, with a same frequency scattering of 0.05~0.15 MHz.

Based on the time series analysis and frequency analysis, it should be considered that the "early part" carried information about micro-cracking with no contamination consists of the first five arrivals. And this "early part" can be used to model AE source functions of dynamic cracks.

4.2. AE Source Functions

As shown in Eqs. (12) and (13), it is possible to model AE source function $f(t)$ by de-convolution of the detected signal $V(t)$ with the Green's function G. The theoretical Green's function of a structure extending infinitely in surface and thickness was given in Eq. (8). Because the de-convolution process is highly sensitive to noise present in AE signals, signals should be forward simulated using the modeled AE source function, to verify the validity of the obtained source function. The forward simulation can be done based on Eq. (11), by the convolution of cubic differential of modeled AE source function with Green's function G.

AE Source functions of dynamic crack simulated by S_1, S_2, S_3 were modeled and presented in Fig. 6.(a), Fig. 7.(a) and Fig. 8.(a), respectively. AE waveforms were forwarded simulated and compared

with the experimental waveforms in Fig. 6 (b), Fig. 7 (b) and Fig. 8 (b). Nearly perfect agreements between forward simulation (solid line) and experiment (dash line) signals were got. The agreements confirmed that numerical calculation for de-convolution of the source functions was correct and the modeled AE source functions were representations for crack stress variation in the transient processes of the simulated crack growth.

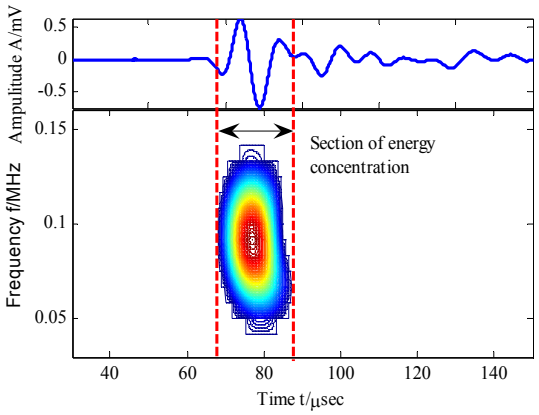

(a)

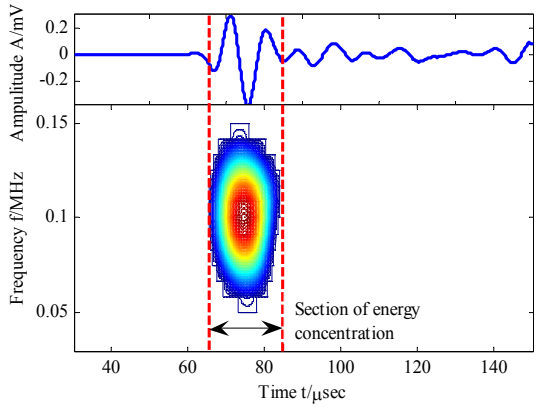

(b)

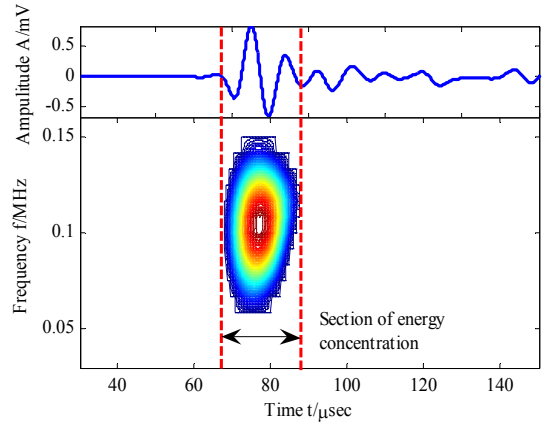

(c)

Fig. 5. STFT for signals from (a) S_1, (b) S_2, and (c) S_3.

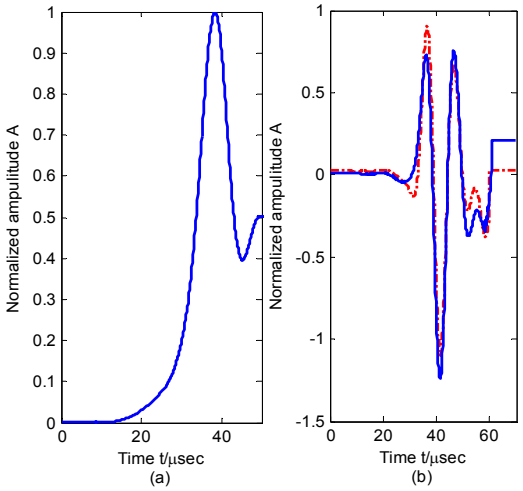

Fig. 6. De-convolution for S_1 of 0.3 mm (a) Modeled AE source function, and (b) Comparison between the forward simulated and detected signal.

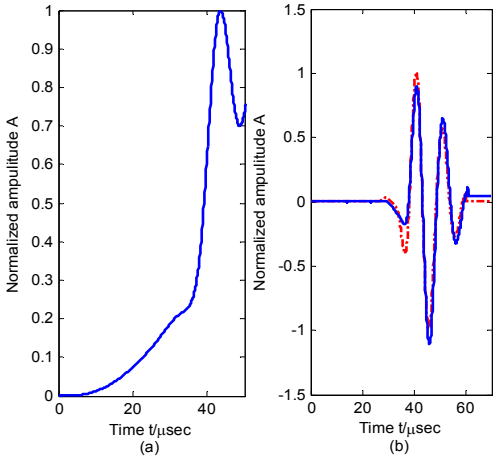

Fig. 7. De-convolution for S_2 of 0.5 mm (a) Modeled source function, and (b) Comparison between the forward simulated and detected signal.

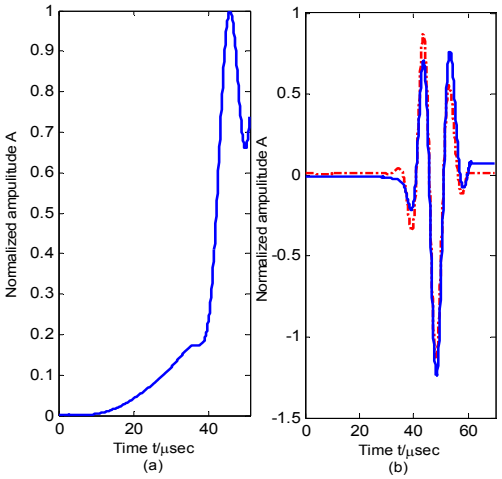

Fig. 8. De-convolution for S_3 of 0.7 mm (a) Modeled source function, and (b) Comparison between the forward simulated and detected signal.

4.3. Mechanisms of Dynamic Crack

The modeled AE source functions of the three dynamic cracks were compared in Fig. 9, which presents the crack stress variation in the process of crack growth. In Fig. 9, each curve starts from point A (7.9 μsec) approaching linearly to $A_i, i=1,2,3$ for a time t_{0i} ; then quickly arrives at a peak P_i for a rise time t_{ri} ; and finally gets to a valley V_i with a decline time t_{di} forming a pulse. The pulse indicates that the crack growth was a transient phenomenon resulting from a combination of complicated processes. In this paper, the combination will be discussed in the aspects of crack initiation and propagation.

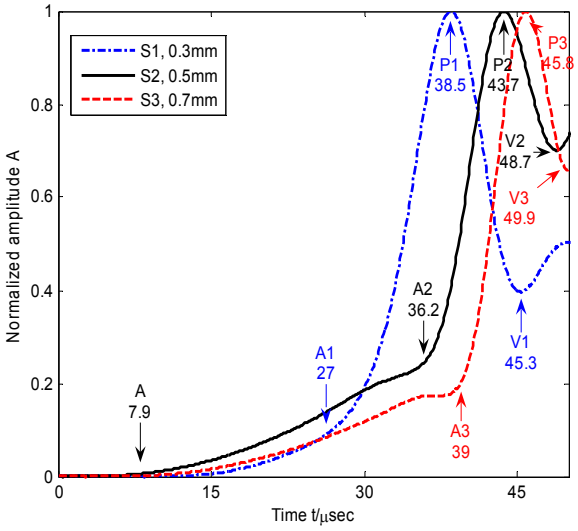

Fig. 9. Comparison of Source functions of S_1, S_2, S_3 .

4.3.1. Crack Initiation Process

In the crack initiation process, the stress in the crack zone should be big enough to induce the crack tip formation. The crack stress variation in the process of crack initiation has been studied and theoretically described as a step-like function [13-14]. The step-like function can be expressed as Eq. (14) with finite duration t_r , and is shown in Fig. 10. The trace in

$$\ddot{f}(t) = -\cos^3\left(\frac{\pi}{t_r}t-\frac{\pi}{2}\right)\sin\left(\frac{\pi}{t_r}t-\frac{\pi}{2}\right)(0\le t\le t_r) \quad (14)$$

Fig. 10 is found to agree well with the section between A_i and P_i in Fig. 9. The agreement suggests that the section from A_i to P_i reproduces the variation of stress in the process of crack initiation. The duration of the section are defined as rise time t_{ri} , which are 11.5 μsec , 7.5 μsec and 6.8 μsec , respectively, for dynamic crack simulated by 0.3 mm, 0.5 mm and 0.7 mm diameter pencil-lead breaking. The rise times exhibit to be lead diameter dependent; and a larger rise time for smaller lead diameter.

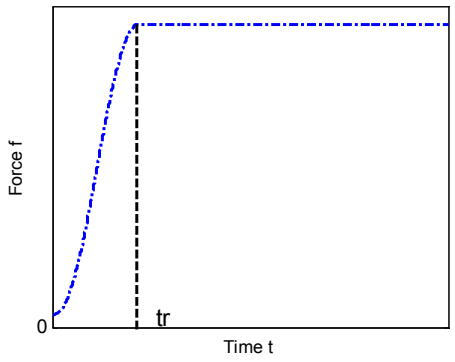

Fig. 10. Step-like function.

4.3.2. Crack Propagation Process

After initiation, the crack propagates with a certain velocity and the stress concentrated in the crack zone was unloaded. This can be observed in the duration of decline time t_{di} from P_i to V_i when the amplitude of AE source function declines. Thus, it is confident to relate the decline time t_{di} to the process of crack propagation.

The decline time of dynamic crack simulated by 0.3 mm, 0.5 mm and 0.7 mm diameter pencil-lead breaking are 6.8 μsec , 5 μsec and 4.1 μsec , respectively. They are the time required for cracking i.e. the time for a crack propagating along a radial of the pencil-lead. Thus, the measured decline time t_{di} can be given as

$$t_{di} = \frac{D_i}{\bar{v}}, i=1,2,3, \quad (15)$$

where $\bar{v}$ is the average crack propagation velocity. Conversion of Eq. (15) yields the average crack propagation velocity, $\bar{v}$ to be

$$\bar{v} = \frac{\bar{D}}{\bar{t}_d} = \frac{D_1+D_2+D_3}{t_{d1}+t_{d2}+t_{d3}}, \quad (16)$$

The velocity of crack propagation is determined as 0.0943 mm μsec^{-1} .

Theoretical treatments of crack propagation predicted the Rayleigh surface wave velocity c_p to be the maximum velocity for the extension of a single straight running crack. Usually a crack develops and propagates at a velocity less than c_p . The terminal crack velocity in glass was reported to be v =1.8

mm μsec^{-1} =0.33 c_p in Kolsky and Rader's experiment employing high-speed photography. Crack branching at a critical stress intensity factor for branching was reported to be v =1.58 mm μsec^{-1} =0.27 c_p in brittle material by Field [15]. The substitution of the surface wave velocity of the graphite c_p =2.4 mm μsec^{-1} [16], results in the crack propagation velocity v =0.039 c_p in this work, which is a reasonable value compared with that in the two above researches for brittle material.

5. Conclusions

Theoretical representation of AE wave motions in steel structure has been studied. At the beginning, AE wave motion was discussed based on elasto-dynamics, and AE waveform was explained as displacement motion due to elastic disturbance such as body forces, surface tractions and displacements. Navier's equation governing AE wave motion was presented, which was then solved using Green's function method. Employing the method, AE waveform was forward modeled by a convolution of AE source function with Green's function. Consequently AE source function was inversely and theoretically modeled from the observed AE signals by a de-convolution procedure. The modeling method was then employed by an experimental study to recover the source function of dynamic crack in steel structure.

In the experimentation, dynamic cracks were simulated on the surface of the steel structure using pencil lead (of 0.3 mm, 0.5 mm, 0.7 mm in diameter) break. In order to overcome difficulties of signal noise and wave reflection, a big and thick steel structure was used; AE signals were captured and recorded through a 20~100 kHz band pass filter; "early part" was determined based on time series analysis and time-frequency analysis.

Based on the modeling method and the "early part" of AE signals, AE source functions related to crack stress variation during crack growth was modeled. According to the AE source functions, mechanisms are summarized as follows:

1) The rise time t_{ri} and decline time t_{di} of the function should be related to the process of crack initiation and propagation, respectively;

2) The rise times exhibit to be crack size dependent; a larger rise time for smaller lead diameter;

3) The average crack propagation velocity of the simulated crack was 0.0943 mm μsec^{-1}, 0.039 c_p.

In this paper, we have shown that theoretical treatments of waveform analyses can be applied to investigating relations between source mechanisms and AE wave motions. The modeling method is unique for monitoring the dynamic processes of crack growth or damage evolution. This research will lead to a better understanding of the cracking or fracture process and the mechanisms of damage growth in materials.

Acknowledgements

This work described in the paper was supported by National Natural Science Foundation of China (No. 51175401 and No.51205230).

References

[1]. V. Lazarus, Perturbation approaches of a planar crack in linear elastic fracture mechanics: A review, *Journal of the Mechanics and Physics of Solids*, Vol. 59, 2011, pp. 121-144.

[2]. J. G. Harris, J. Pott. Surface Motion Excited by Acoustic Emission From a Buried Crack, *Journal of Applied Mechanics*, Vol. 51, 1984, pp. 77-836.

[3]. Eric N. Landis, Surendra P. Shah. Recovery of microcrack parameters in mortar using quantitative acoustic emission, *Journal of Nondestructive Evaluation*, Vol. 12, Issue 4, 1993, pp. 219-232.

[4]. H. N. G. Wadley and C. B. Scruby, A study of deformation and fracture process in a low-alloy steel by acoustic emission transient analysis, *Acta Metallurgica*, Vol. 27, 1979, pp. 613-625.

[5]. T. Jayakumar, C. K. Mukhhopadhyay, and S. Venugopal et al., A review of the application of acoustic emission techniques for monitoring forming and grinding processes, *Journal of Materials Processing Technology*, Vol. 159, 2005, pp. 48-61.

[6]. C.-S. Kao, F. C. S. Carvalho, and J. F. Labuz, Micromechanisms of fracture from acoustic emission, *International Journal of Rock Mechanics & Mining Sciences*, Vol. 48, 2011, pp. 666-673.

[7]. C. L. Pekeris, The Seismic Surace Pulse, *Geophysics*, Vol. 41, 1955, pp. 469-480.

[8]. J. E. Michaels, T. E. Michaels, and W. Sachse, Applications of De-convolution to Acoustic Emission Signal Analysis, *Materials Evaluation*, Vol. 39, Issue 11, 1981, pp. 1032-1036.

[9]. C. U. Grosse and Masayasu. Ohtsu, Acoustic Emission Testing, *Springer-Verlag*, 2008.

[10]. S. Yuyama, T. Imanaka, and M. Ohtsu, Comparison between experimentally detected surface motions due to a disbanding stainless overlay and simulated waveforms, *Nuclear Engineering and Design*, Vol. 94, Issue 3, 1986, pp. 345-355.

[11]. D. W. Vasco, Deriving source-time function using principal component analysis, *Bulletin of the Seismological Society of Americ*a, Vol. 79, Issue 3, 1989, pp. 711-730.

[12]. Lulian Marinescu, Dragos Axinte, A time-frequency acoustic emission-based monitoring technique to identify workpiece surface malfunctions in milling with multiple teeth cutting simultaneously, *International Journal of Machine Tools and Manufacture*, Vol. 49, Issue 1, 2009, pp. 53-65.

[13]. Masayasu Ohtsu, Source mechanism and waveform analysis of acoustic emission in concrete, *Journal of Acoustic Emission*, Vol. 1, Issue 2, 1982, pp. 103-112.

[14]. Masayasu Ohtsu, Takahisa Okamoto, and Shigenori Yuyama, Moment Tensor Analysis of Acoustic

Emission for Cracking Mechanisms in Concrete, *ACI Structural Journal*, Vol. 95, Issue 2, 1998, pp. 87-95.

[15]. Young H. Kim and H. C. Kim, Source function determination of glass capillary breaks, *Journal of Physics D: Applied Physics*, Vol. 26, Issue 2, 1993, pp. 253-258.

[16]. P. Karthikeyan, V. K. Ravindran, and Abilash et al., Prediction of erosion characteristics for ablative throat insert liners using ultrasonic velocity measurements, in *Proceedings of the National Seminar & Exhibition on Non-Destructive Evaluation*, 2011, pp. 167-170.

2013 Copyright ©, International Frequency Sensor Association (IFSA). All rights reserved.
(http://www.sensorsportal.com)